Selectively laser-melted aluminum alloy's resistance to fatigue during T6 heat treatment

Asis Kumar Nayak
College of Engineering Bhubaneswar, Bijupatnaik University of Technology, Bhubaneswar, Odisha

Abstract

It is vital to evaluate the fatigue resistance of the material that makes up manufactured parts before certification because of the intricate microstructure and defects that are carried over from this ALM process. This work is specifically addressing this problem, with a focus on the influence of flaws and microstructural factors on fatigue life. Two configurations of specimens (0° and 90°) were constructed in order to assess the effect of the produced microstructure anisotropy on fatigue characteristics. The defect population was characterized by size using X-ray 3D tomography. Four additional characteristic scales [1-3] are taken into account when characterizing microstructure: melt-pools, crystallographic grains, dendritic structure, and precipitates. S-N curves for as-built and heat-treated samples are established for R= -1 in order to determine the fatigue properties. Using Kitagawa type diagrams, the defect size that initiates fatigue damage in each sample is identified in order to establish a relationship between the defect size and the fatigue limit. It is demonstrated that, in terms of fatigue resistance, defect size is the first order characteristic. We are able to measure the increase in fatigue resistance brought about by the peak hardening treatment by using the Kitagawa diagrams for both as-built and heat-treated samples.

Keywords: Fatigue, Defect size, AlSi10Mg, ALM, Microstructure, T6.

1. Introduction

Since additive manufacturing makes it possible to produce parts with complicated geometry and topographic optimization, it is thought to be a revolutionary process compared to previous methods. In the context of aeronautics, realizing the parts entails them qualifying, which is the comprehension of the fatigue behavior resulting from material integrity. Therefore, to quantify the effect of each material parameter on the fatigue behavior of such parts, knowledge of the material's microstructure as well as metallurgical flaws inherited from the manufacturing process is required. Consequently, it will be feasible to work toward process optimization with reference to tiredness behavior. This study discusses an aluminum alloy that is hypoeutectic and was created via the ALM process. Studies on the microstructural characterisation, flaws, and anisotropy effects resulting from the specimens' growth direction in connection to static mechanical characteristics such UTS, Ys, and Ef have been conducted [3, 4]. In reference to fatigue, Brandl et al. [5] demonstrated that anisotropy resulting from production direction can be observed at a platform temperature of 30 °C. The previous author claims that when a T6 heat treatment and a platform temperature of 300°C are combined, the direction of sample growth no longer differs. In their evaluation of the effect of T6 treatment on fatigue performance for as-built manufacturing surfaces, Maskery et al. [6] found that T6 treatment significantly increased the fatigue limit. The specimens machined from the T6 heat-treated bars exhibit a higher fatigue resistance, according to Aboulkhair et al. [7]. There aren't many studies that measure how faults affect the fatigue limit. This study aims to assess the effect of defect size on the fatigue limit with and without T6 using Kitagawa type diagrams.

2. Experimental approach

2.1. Material and samples

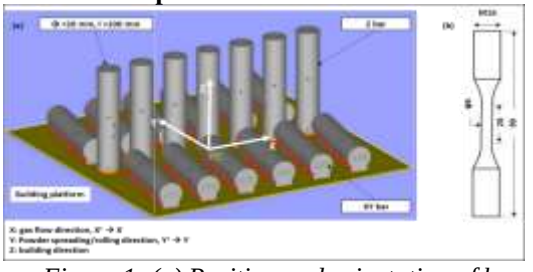

Figure 1: (a) Position and orientation of bar, (b) machined fatigue test specimen

Two distinct productions of AlSi10MgSi by SLM, noticed P1 and P2, were considered in the present study.
Firstly, a PHENIX PM100 developed by 3D SYSTEMS was used for the P1 production using TLS powder. This machine is equipped with a 200W fiber laser YAG. The layering is done by means of a roller. All P1 specimens have been removed from XY bars built on an aluminum platform at 200°C. In order to relax the stress due to the process, a post processing heat treatment have been performed during one hour at 160°C. The P1 specimens were tested on a rotative bending machine. The results of the P1 production tests were analyzed and used as a reference for the study. Secondly, the P2 samples were built on a platform at 200°C using EOS M290 machine and EOS powder. This machined is equipped with a 400 W fiber laser, and the layering is performed by means of a scraper. A stress relaxation treatment have been performed during 2 hours at 300°C. Both powders used for P1 and P2 have chemical compositions in accordance with standard NF EN 1706:2010. P2 samples have been built in two directions, namely XY and Z as in ***figure 1-a***. Fatigue specimens test have been machined (MA) from the produced bars by fine turning. Fatigue test specimens geometry is given on ***figure 1-b***. After machining, some specimens have been subjected to heat treatment T6 with specific conditions in ***table 1***.

Table 1: conditions du T6

Steps	Temperature (°C)	Duration (h)	Environnement
Solid solutioning	540	8	Air
Quenching	20		Water
Tempering 1	20	24	Air
Tempering 2	160	10	Air
Cooling to room temperature			

This investigation leads to a description of the microstructure along four main characteristics parameters, namely:

- The melt-pools that can be geometrically characterized by them length, width and height, and which reflect the impression left by the laser during the melting of the deposed powder. As shown in ***figure2-a***, these melt-pools are strongly anisotropic in shape. Measurements of the melt-pool dimensions have been performed on those melt-pools by images analysis and the mean values are (600; 150; 80) corresponding to (length, width and height). A fine study of the interior and of the boundaries of the melt-pools by Kempen et al **[1]** has shown that those melt-pools are constituted of the heterogeneous distribution of eutectic silicon in the alpha-phase aluminum. In ***figure2-b*** it can further be noticed that, after heat treatment, the melt-pool boundaries are no longer visible, presumably due to the diffusion and dissolution of the silicon in the aluminum matrix. According to Li et al **[2],** the higher the solution temperature, the coarser are the silicon particles typically around 2 to 4 µm within a range of 450°C to 550°C. Additional growth of these particles is achieved during artificial aging.

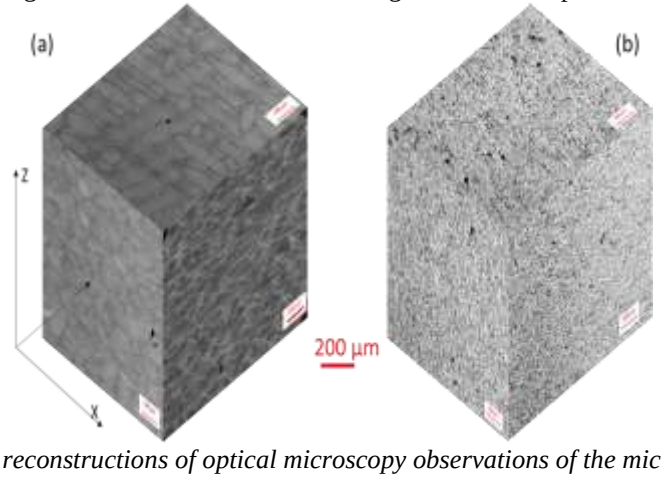

Figure 2: 3D reconstructions of optical microscopy observations of the microstructures after surface polishing, without etching, (a): without heat treatment (b): after T6

- The dendritic structure is geometrically characterized by the diameter of the eutectic silicon observed from the scanning plan, and by the distance between two fibrous eutectic silicon seen from transversal plans. The rapid solidification involved in SLM process does not allow the formation of the dendritic structure with secondary

arms as it is the case for cast aluminum alloy **[8]**. Therefore, in this study, a Dendritic Arm Spacing DAS

dimension of about 0.5 to 2 µm was determined, which is significantly smaler compared to the characteristic SDAS parameter in cast aluminum alloys (30 to 100µm function of cooling rate). Previous studies have shown that this parameter has a large influence on the fatigue behavior **[8, 9]**. Typically, according to Wang et al **[9,]** in absence of defect, the finer the SDAS, the higher is fatigue life. As previously mentioned, the melt-pools are decorated by eutectic phases. Many studies **[1, 2, 11]** agree on the point that this silicon distribution reveals the dendritic structure of the alloy.

- Crystallographic grain orientations have not been characterized using EBSD technique. However, according to Lore et al **[1],** grains are strongly anisotropic in term of geometry and textured with an epitaxial growth. It is also important to mention that the grain growth can encompass one to three melt pools, reflecting the size of powder bed. According to Wang et al **[10]**, the peak hardening treatment does not affect the size and shape of grains. Therefore, in this study we will consider that the grains are not affected after T6 treatment.
- Silicon precipitates and iron rich needles mostly appears after T6. In fact, during the heat treatment, diffusion and segregation of Si and Fe atoms occurs, leading to the formation of Fe-rich precipitates and Si crystals randomly distributed in the Al-matrix. A quantitative study of precipitates have been performed on a thin foil removed from a heat treated samples by FIB milling. TEM analysis of this foil shows the presence of twinned silicon grains with 98% of silicon for only 2% of aluminum, Fe-rich (10/41/49 - Fe / Al / Si) needles, mostly β-Al7FeSi2 and β-Al6Fe2Si2 compounds, and large mono-crystalline aluminum grains oriented along [112] and [114] directions.

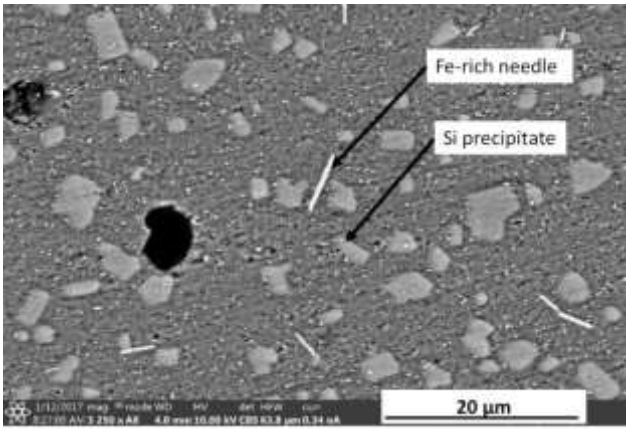

Figure 3: SEM (SEI) observation of the T6 microstructure (polish, without etching): precipitation structure and intermetallics needles

2.2. Defect characterization in relation with the process parameters

Different techniques can be carry out to characterize the defects in a sample in terms of defect type, size, morphology and location. Firstly, it is possible to use optical microscope on a cross section previously polished. However this method can bring several errors induced by the preparation of samples, especially cutting and polishing. An alternative method could consist in observing a fracture surface after completion of a fatigue test for example. The principal advantage of this method lies on the fact that the critical defect and its location are a posteriori determined. By observing fracture surfaces such as in ***figure 6***, two main families of defects inherited to SLM process are evidenced:

- The gas pores, characterized by a spherical shape. These defects are due to the interaction between the laser beam and the powder bed, especially for high laser power and low scanning speed.
- The unmelted particles and/or lack of fusion characterized by a complex geometry. Those defects are mainly related ue to the layering process and also to the projection of molten metal droplets onto the powder bed. The droplets then covers unmelted particles and increases the energy required to melt them as the unmelted particles below.

However the observation of a fracture surface means the lost of a lot information about the critical defect. Thus, a deterministic method is required to collect all information on a given defect present in a given specimen. As a consequence, the X-ray tomography have been used here. .

In this technique, the specimen is fixed to a rotating support and it is then subjected to an X-ray beam. A screen

collects the more or less attenuated signal in relation with the local permeability of the material. Several images are then taken where it is possible to observe a contrast and brightness corresponding to the presence or absence of defects. By After a post-treatment using Avizo® software package, all images are binarized and a segmentation is done so that it is possible to reconstitute defects as ***figure 4-a***. As shown in ***figure 4-b***, the defect size distribution lies the 28 to 52 µm range. As it can be seen on fracture surface, the fatal fatigue crack is due to a defect that is clearly the bigger contained by the samples. Which means the fatigue is not sensitive to all the defect population but to the bigger one.

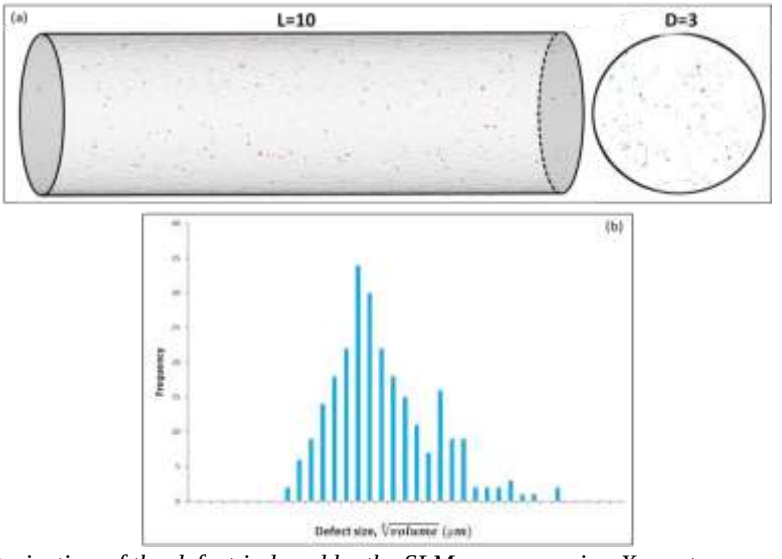

Figure 4: (a) Characterization of the defect induced by the SLM process, using X-ray tomography with a resolution of 5µm per voxel (b) defect size distribution

2.3. Fatigue test

In this study cylindrical specimens were used as shown on ***figure 1-c***. Fatigue tests have been performed at room temperature on resonance machine with a load ratio R=-1. The frequency was in the range of 80 to 82 Hz.

2.4. Determination of the fatigue limit

The fatigue limit have been defined at one million cycles. A step by step method described by Iben Houria **[12]** have been used as it is the only way to evaluate the fatigue limit for a natural defect. It is assumed that no significant damage is introduced in the loading as shown by Roy et al [**13]** for cast alloy A356. The failure is define by a 5Hz drop of frequency. The fatigue limit is then determined for each specimen after failure according to the following method:

3. Results and discussions

The analysis of the fatigue test is focused on the anisotropic effects due to the process. The effect of anisotropy induced by the building strategy (XY versus Z) will be examined on the basis of S-N curves for machined and machined plus T6. Secondly, for same samples configurations, Kitagawa-type diagrams are considered to quantify the effect of defect size on fatigue limit.

3.1. S-N curves

Even though the microstructure is strongly anisotropic in non-heat-treated samples, no difference is noticed between XY and Z samples in terms of fatigue life. The Basquin curves indicate a slight anisotropy effect between XY and Z samples. On the ***figure 5*** the S-N curves of P2 machined and heat treated samples are compared. The fatigue limit is estimated using an extrapolation with least square method. A 20% augmentation in fatigue limit is observed between P2-XY-MA and P2-XY-MA-T6 while more than 45% is observed for Z samples. Compared to P1-XY-MA the fatigue limit at one million of cycle of P2-XY-MA is improved by about40%. The fracture surface examination in ***figure 6*** furthermore suggests that a significant increase of fatigue limit between P1 and P2 is primarily due to a reduction in the critical defect size. For all P2 specimen containing similar defects, an increase of fatigue limit is noticed after T6 despite the presence of iron needles which are supposed to degrade the fatigue crack initiation tolerance **[14]**. That increase observed after heat treatment is due to the strengthening of the matrix via the applied T6. However it is observed that a peak hardening treatment leads to a more pronounced anisotropy effect between

XY and Z orientations.

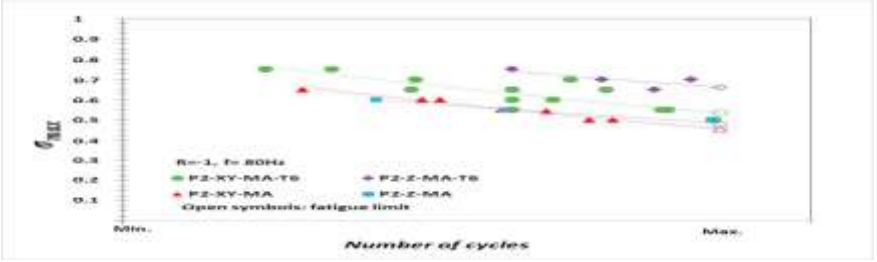

Figure 5: effect of building direction on fatigue life for as-built and T6 samples.

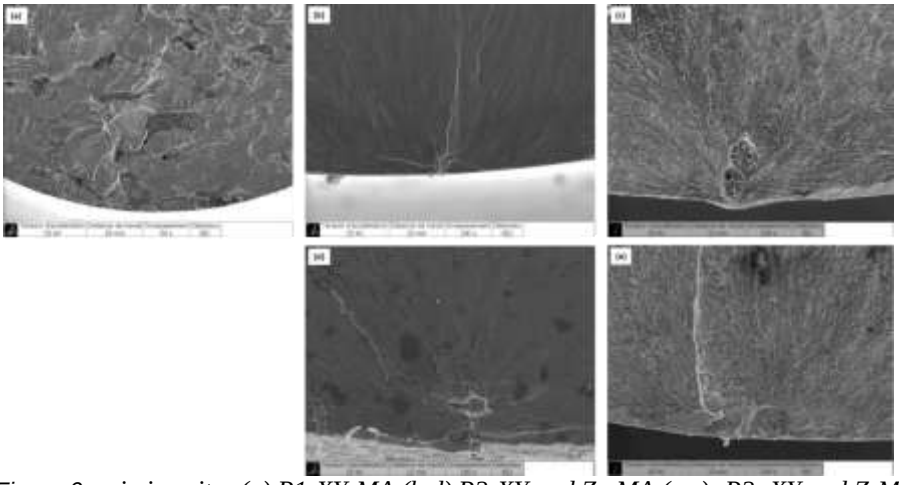

Figure 6: priming sites (a) P1-XY-MA (b,d) P2-XY and Z –MA (c,e): P2: XY and Z-MA-T6

3.2. Kitagawa diagram

The examination of the fracture surfaces indicates that the fatigue failure is mostly controlled by initiation on metallurgical defects inherited from the ALM process. In order to plot the Kitagawa type diagram, defect size

have been assessed using Murakami's parameter $\sqrt{area}$. Moreover ***Figure 7*** explains the criterion used to define the defect size according to **[15].** In ***figure 8*** the fatigue limit is plotted as a function of the defect size measured on fracture surfaces. In order to extend the range of this study, spherical artificial defects were introduced by electro discharge machining (EDM). For both types of microstructure, i. e. none and peak-hardened, even in presence of defects, the Kitagawa-type diagram shows that the fatigue limit is sensitive to defect size; it also confirms the observation on anisotropy made on S-N curves. For P2-XY/Z-MA the fatigue limit is controlled by the defect size beyond a certain defect size while in the T6 microstructure, the concept of defect free material seems not yet acquired. As a consequence under a critical defect size the fatigue life is controlled by the precipitation structure and the defects. Furthermore, ***figure 8*** shows there is no influence of defect type and all the trends curves seems to converge for big defect.

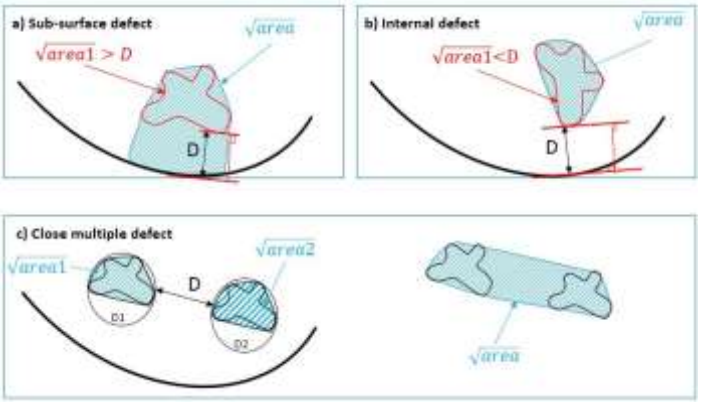

Figure 7: assumption for the assessment of the defect size

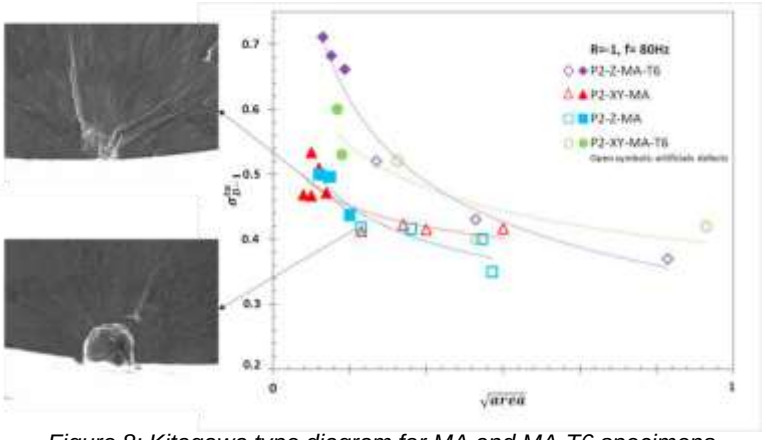

Figure 8: Kitagawa type diagram for MA and MA-T6 specimens

4. Conclusions

Five primary scales were used in this investigation to characterize the AlSi10Mg material both before and after T6.
• Melt-pools, measuring 600 x 150 x 80 μm3, vanish following T6;
The precipitation structure, crystallographic grains, and cells, α or DAS (0.5 to 2 μm):
silicon precipitates (4 to 10 μm), which increase in number after T6;
The FeSi needles, which emerge subsequent to T6; • Process-inherited defects. To comprehend how the microstructure affects fatigue behavior, the fatigue limit has been measured. The following exhaustion outcomes followed as a result:

• An isotropy between XY-MA-T6 and Z-MA-T6 is detected; • Anisotropy between defect size and production direction is absent for the same defect size in non-heated material; • Fatigue strength is enhanced by matrix improvement by T6 heat treatment in the presence of defects.
Kitagawa type diagrams have been used to quantify the impact of defect size. The following findings were noted: • The type of defect has no effect on the fatigue limit; • The critical defect size resulting from the process has been quantified; • There is a defect size threshold beyond which the fatigue limit is solely controlled by the defect size; below that threshold, the fatigue limit is controlled by both the defect size and the microstructure.

References

[1]: L. Thijs, K. Kempen, J.P. Kruth, J. V. Humbececk, Fine-structured aluminium products with controllable texture
by selective laser melting of pre-alloyed AlSi10Mg powder, Acta Materialia 61(2013) 1809-1819
[2]: Wei Li, Shua Li, Jie Liu, AngZhang, Yan Zhou, Qingsong Wei, Chunze Yan, Yusheng Shi, Effect of heat treatment on AlSi10Mg alloy fabricated by selective laser melting: Microstructure evolution, mechanical properties and fracture mechanism, Material Science & Engineering A 663 (2016) 116-125
[3]: Nesma T. Aboulkhair, Ian Maskery, Chris Tuck, Ian Ashcroft, Nicola M. Everitt, The microstructure and mechanical properties of selectively laser melted AlSi10Mg: the effect of a conventional T6-like heat treatment, Material Science & Engineering A 663 (2016) 139-146
[4]: K. Kempen, L.Thijs, J. Van Humbeeck and J.-P. Kruth, Mechanical properties of AlSi10Mg produced by

Selective Laser Melting, Physics Procedia 39 (2012) 439 – 446
[5]: Erhard Brandle, Ulrike Heckenberger, Virtus Holzinger, Damien Buchbinder, Additive manufactured AlSi10Mg samples using Selective Laser Melting (SLM): Microstructure, high cycle fatigue, and fracture behavior, Material and Design 34 (2012) 159-169
[6]: I. Maskery, N. T. Aboulkhair, C. Truck R.D. Wildman, Fatigue performance enhancement of selective laser melted aluminium alloy by heat treatment
[7]: Nesma T. Aboulkhair, Ian Maskery, Chris Tuck, Ian Ashcroft, Nicola M. Everitt, Improving the fatigue behaviour of a selectively laser melted aluminium alloy: Influence of heat treatment and surface quality, Material and Design 104 (2016) 174-182
[8]: Mohamed Iben Houria, Yves Nadot, Raouf Fathallah, Matthew Roy, Daan M. Maijer, Influence of casting defect and SDAS on the multiaxial fatigue behaviour
of A356-T6 alloy including mean stress effect, International Journal of Fatigue 80 (2015) 90–102
[9]: Q.G. Wang *, D. Apelian, D.A. Lados, Fatigue behavior of A356-T6 aluminum cast alloys. Part I. Effect of casting defects, Journal of Light Metals 1 (2001) 73-84
[10]: JIANG Wen-ming, FAN Zi-tian, LIU De-jun, Microstructure, tensile properties and fractography of A356 alloy under as-cast and T6 obtained with expendable pattern shell casting process, Trans. Nonferrous Met. Soc. China 22(2012) s7−s13
[11]: Tang Ming, Inclusion, porosity, and Fatigue of AlSi10Mg Parts Produced by Selective Laser Melting (2017) Dissertation. 903
[12]: Mohamed Iben Houria, Experimental investigation and modeling the fatigue life of a cast aluminium alloy A356-T6 under multiaxial loading (2015) Dissertation
[13]: M. Roy, Y. Nadot, C. Nadot-Martin, P.-G. Bardin, and D. Maijer, "Multiaxial Kitagawa analysis of A356-T6," *International Journal of Fatigue*, vol. 33, pp. 823-832, 2011.
[14]: J. Yi, Y. Gao, P. Lee, and T. Lindley, "Effect of Fe-content on fatigue crack initiation and propagation in a cast aluminum–silicon alloy (A356–T6)," *Materials Science and Engineering: A*, vol. 386, pp. 396-407, 2004.
[15]: Y. Murakami and M. Endo, "Effects of defects, inclusions and inhomogeneities on fatigue strength," *International Journal of Fatigue*, vol. 16, pp. 163-182, 1994.